JOURNAL OF COMPUTATIONAL PHYSICS **131,** 323–326 (1997)
ARTICLE NO. CP965598

Solution of the Poisson Equation in an Annulus

Ivar Christopher,* George Knorr,* Magdi Shoucri,† and Pierre Bertrand‡

*Department of Physics and Astronomy, University of Iowa, Iowa City, Iowa 52242; †Hydro-Québec, Varennes, Québec, Canada J3X 1S1; ‡LPMI-URA 835 CNRS, Université de Nancy I, France

Received February 5, 1996; revised May 28, 1996

A simple method is described to solve Poisson's equation in an annulus using conformal mapping and fast Fourier transforms.

We communicate a method to solve the Poisson equation in an annulus which is fast and convenient because it allows the application of the standard fast Fourier transform (FFT). The problem arises, e.g., in the context of modelling the scrape-off layer in a tokamak plasma when the plasma is no longer charge neutral.

We assume a circular domain between radii r_0 and r_1 and let the boundary condition of the potential be given by

$$\phi(r_0) = \phi_0, \quad \phi(r_1) = \phi_1. \tag{1}$$

The equation to be solved is

$$\nabla^2\phi(r, \varphi) = -\rho(r, \varphi). \tag{2}$$

Expanding in angular modes,

$$\begin{Bmatrix} \phi(r, \varphi) \\ \rho(r, \varphi) \end{Bmatrix} = \sum_m \begin{Bmatrix} \phi_m \\ \rho_m \end{Bmatrix} e^{im\varphi},$$

we obtain

$$\frac{\partial^2\phi_m}{\partial r^2} + \frac{1}{r}\frac{\partial\phi_m}{\partial r} - \frac{m^2}{r^2}\phi_m = -\rho_m(r),$$

which has the solution

$$\phi_m(r) = \int_{r_0}^{r_1} dr' G_m(r, r')\mu_m(r').$$

The Green function $G_m(r, r')$ is given by

$$G_m(r, r') = \frac{1}{2m[(r_1/r_0)^m - (r_o/r_1)^m]} \begin{cases} u_1^m(r')u_0^m(r), & r < r', \\ u_0^m(r')u_1^m(r), & r > r', \end{cases}$$

with

$$u_0^m = \left(\frac{r}{r_0}\right)^m - \left(\frac{r}{r_0}\right)^{-m}, \quad u_1^m = \left(\frac{r}{r_1}\right)^m - \left(\frac{r}{r_1}\right)^{-m};$$

$$G_0(r, r') = \frac{1}{\ln(r_1/r_0)} \begin{cases} \ln\left(\frac{r'}{r_1}\right)\ln\left(\frac{r}{r_0}\right), & r < r', \\ \ln\left(\frac{r'}{r_0}\right)\ln\left(\frac{r}{r_1}\right), & r > r'. \end{cases}$$

Whereas the solution is in principle simple and straightforward, no fast numerical algorithm is known to the authors which would be comparable to an FFT in Cartesian coordinates.

A better approach is to use conformal mapping. The general principle of conformal mapping and application to two-dimensional practical problems is described extensively by Henrici [1]. Goedbloed [2, 3] for example reduced an equilibrium and stability problem of a tokamak plasma to the solution of the Laplace equation with free boundaries and solved it by conformal methods.

Here we solve the Poisson equation in an annulus (in the z-plane) by mapping it into a rectangular area (in the w-plane) by the complex function $w(z) = u(x, y) + iv(x, y)$. Then (2) is transformed into

$$\left[\frac{\partial^2}{\partial u^2} + \frac{\partial^2}{\partial v^2}\right]\phi(u, v) = -\left|\frac{dz}{dw}\right|^2 \rho(u, v), \tag{3}$$

and in the rectangular domain of the u-v-plane an FFT can be used. This equation is still very general because $z(w)$ has not been specified. Prescribing the potentials on all four sides of the rectangle, arbitrary singly connected domains can be mapped into the rectangle. Imposing periodic boundary conditions on two (opposite) sides and prescribing the potential on the other sides, doubly connected domains map into the rectangle. We confine ourselves here to the simple case of an annulus; other cases can be solved in an analogous manner. For an annulus we

0021-9991/97 $25.00

choose $w(z) = \ln z - \ln r_0$ with $z = x + iy = r \exp(i\varphi)$, resulting in

$$u = \ln\left(\frac{r}{r_0}\right), \quad v = \varphi.$$

An annulus in the x-y-plane with radii r_0, r_1, $r_0 < r_1$ is mapped into a rectangle in the $u - v$-plane, as shown in Fig. 1. With $0 \le u \le u_1 = \ln(r_1/r_0)$, the Poisson equation (3) becomes

$$\left[\frac{\partial^2}{\partial u^2} + \frac{\partial^2}{\partial v^2}\right] \phi(u, v) = r_0^2 e^{2u} \rho(u, v) = -R(u, v) \quad (4)$$

with the boundary conditions (1).

The v-coordinate is periodic so that an expansion

$$\begin{Bmatrix} \phi(u, v) \\ R(u, v) \end{Bmatrix} = \sum_m \begin{Bmatrix} \phi_m(u) \\ R_m(u) \end{Bmatrix} e^{imv}$$

results in

$$\left(\frac{d^2}{du^2} - m^2\right) \phi_m(u) = -R_m(u). \quad (5)$$

$R_m(u)$ is arbitrary and does not necessarily vanish at the boundaries. In order to apply a fast transform, we decompose $R_m(u) = \tilde{R}_m(u) + \bar{R}_m(u)$, where

$$\bar{R}_m(u) = R_m(0) + [R_m(u_1) - R_m(0)] \frac{u}{u_1},$$

so that $\tilde{R}_m(0) = \tilde{R}_m(u_1) = 0$. Writing $\phi_m(u) = \tilde{\phi}_m(u) + \bar{\phi}_m(u)$, Eq. (5) becomes

$$\left(\frac{d^2}{du^2} - m^2\right) \tilde{\phi}_m(u) = -\tilde{R}_m(u) \quad (6)$$

and

$$\left(\frac{d^2}{du^2} - m^2\right) \bar{\phi}_m(u) = -\left[R_m(0) + (R_m(u_1) - R_m(0)) \frac{u}{u_1}\right]. \quad (7)$$

Equation (6) is solved by a fast sin-transform or, reflecting the data at $u = 0$, by an FFT over twice the length:

$$\begin{Bmatrix} \tilde{\phi}_m(u) \\ \tilde{R}_m(u) \end{Bmatrix} = \sum_n \begin{Bmatrix} \tilde{\phi}_{mn} \sin n\pi (u/u_1) \\ \tilde{R}_{mn} \sin n\pi (u/u_1) \end{Bmatrix}. \quad (8)$$

The potential at $u = 0$, $u = u_1$ vanishes for this part of the solution.

Equation (7) is integrated analytically, incorporating the boundary conditions (1), and results in the solutions

$$\bar{\phi}_0(u) = -\frac{1}{2} R_0(0) u^2 + \frac{1}{6u_1} (R_0(u_1) - R_0(0) u^3) - \left[\phi_0(0) - \phi_0(u_1) - \frac{1}{2} R_0(0) u_1^2 - \frac{1}{6} (R_0(u_1) - R_0(0)) u_1^2\right] \frac{u}{u_1} + \phi_0(0),$$

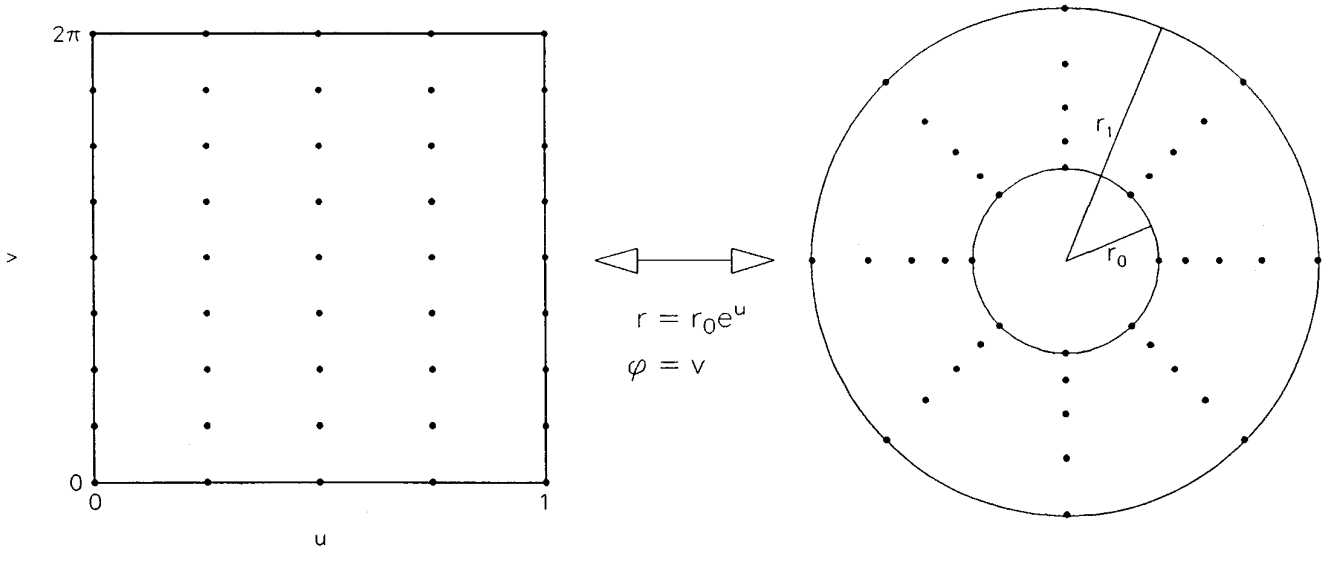

FIG. 1. Conformal mapping of an annulus on a rectangle, showing the grid points for numerical calculation.

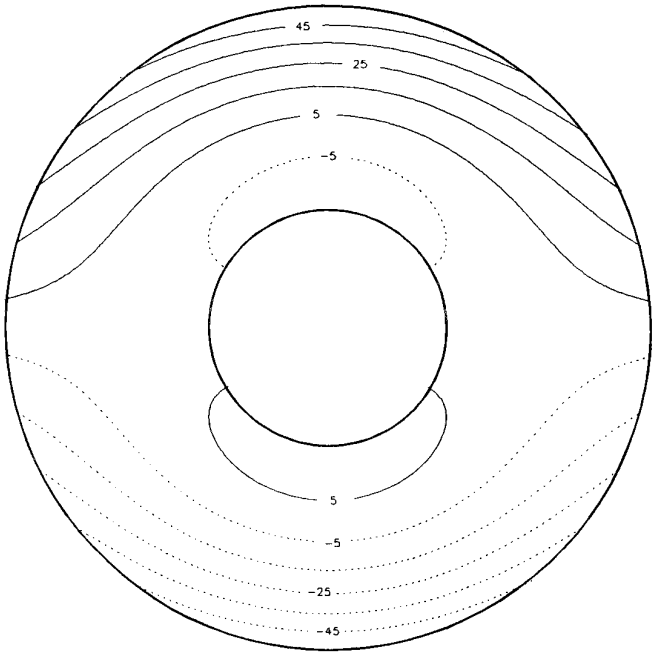

FIG. 2. Contour plot of the charge density used in the numerical example.

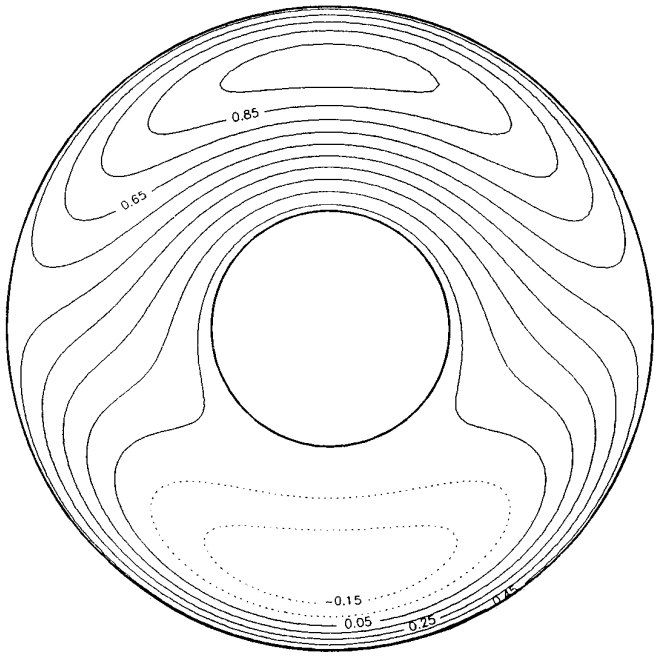

FIG. 3. Potential solution to the charge density of Fig. 2 and the boundary conditions $\phi_0 = \phi(r_0) = 0$, $\phi_1 = \phi(r_1) = 0.5$. Note the asymmetric potential structure caused by the inhomogeneous boundary conditions.

$$\bar{\phi}_m(u) = \frac{R_m(0)}{m^2}\left(1 - \frac{\sinh m(u_1 - u)}{\sinh mu_1}\right) - \frac{R_m(u_1)}{m^2}\frac{\sinh mu}{\sinh mu_1} + \frac{R_m(u_1) - R_m(0)}{m^2}\frac{u}{u_1},$$

for $m \neq 0$.

When transforming back from the $u - v$-rectangle into the r-φ-annulus, the components of the potential (and electric field, if desired) are no longer equidistant in the r-direction, as is seen in Fig. 1, but the distance between points decreases for smaller r-values. From the standpoint of numerical analysis one might wish to see a point distribution such that each point represents the same area. This is not the case here. However, for small aspect ratios the imbalance is insignificant and is a small price paid for being able to use FFTs.

As numerical example we calculate the potential for the charge distribution

$$\rho(r, \varphi) = -\alpha[15r^2 - 8(r_0 + r_1)r + 3r_0r_1] \sin \varphi,$$

as shown in Fig. 2. The resulting exact potential is

$$\phi(r, \varphi) = \alpha[r^4 - (r_0 + r_1)r^3 + r_0r_1r^2] \sin \varphi + 0.5\frac{\ln(r/r_0)}{\ln(r_1/r_0)},$$

with boundary conditions $\phi_0 = 0$, $\phi_1 = 0.5$, as shown in Fig. 3. Figure 4 shows the solution for homogeneous boundary conditions, for which the logarithmic term does not appear. Table I gives the differences between exact and numerical solutions for the inhomogeneous case for (a) an 8×8 and (b) a 16×16 grid. Halving the grid spacing reduces the error by about an order of magnitude.

Solving for the potential on a 128×128 grid takes less than a second on a 90 MHz Pentium PC.

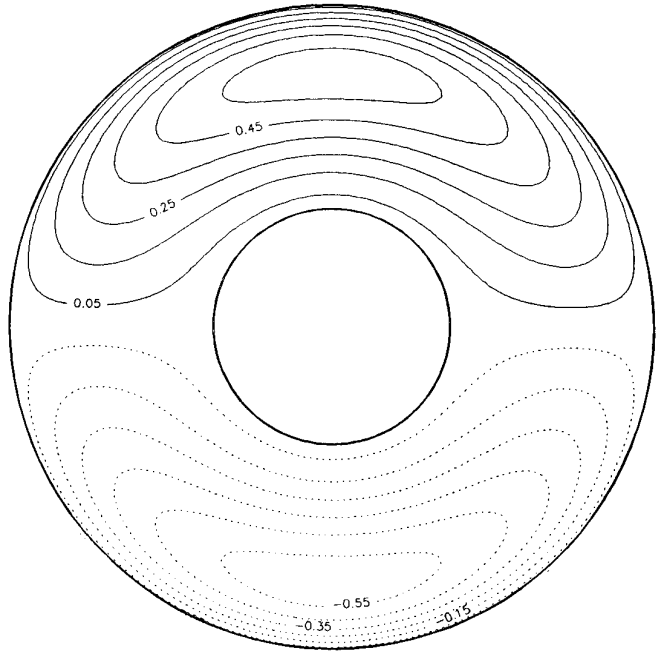

FIG. 4. The same as Fig. 3 but with homogeneous boundary conditions $\phi_0 = \phi_1 = 0$.

TABLE I

The Difference between the Exact and the Numerical Solution at Selected Grid Points for the Potential Shown in Fig. 3

(a)

	φ							
r	0.00	0.79	1.57	2.36	3.14	3.93	4.71	5.50
0.37	0.00E + 0	0.00E + 0	0.00E + 0	0.00E + 0	0.00E + 0	0.00E + 0	0.00E + 0	0.00E + 0
0.42	0.00E + 0	1.24E − 4	1.75E − 4	1.24E − 4	0.00E + 0	−1.24E − 4	−1.75E − 4	−1.24E − 4
0.47	0.00E + 0	2.41E − 4	3.41E − 4	2.41E − 4	0.00E + 0	−2.41E − 4	−3.41E − 4	−2.41E − 4
0.54	0.00E + 0	3.80E − 4	5.38E − 4	3.80E − 4	0.00E + 0	−3.80E − 4	−5.38E − 4	−3.80E − 4
0.61	0.00E + 0	4.90E − 4	6.93E − 4	4.90E − 4	0.00E + 0	−4.90E − 4	−6.93E − 4	−4.90E − 4
0.69	0.00E + 0	6.77E − 4	9.57E − 4	6.77E − 4	0.00E + 0	−6.77E − 4	−9.57E − 4	−6.77E − 4
0.78	0.00E + 0	7.23E − 4	1.02E − 3	7.23E − 4	0.00E + 0	−7.23E − 4	−1.02E − 3	−7.23E − 4
0.88	0.00E + 0	1.19E − 3	1.68E − 3	1.19E − 3	0.00E + 0	−1.19E − 3	−1.68E − 3	−1.19E − 3
1.00	0.00E + 0	0.00E + 0	0.00E + 0	0.00E + 0	0.00E + 0	0.00E + 0	0.00E + 0	0.00E + 0

(b)

0.37	0.00E + 0	0.00E + 0	0.00E + 0	0.00E + 0	0.00E + 0	0.00E + 0	0.00E + 0	0.00E + 0
0.42	0.00E + 0	7.69E − 6	1.09E − 5	7.69E − 6	0.00E + 0	−7.69E − 6	−1.09E − 5	−7.69E − 6
0.47	0.00E + 0	1.54E − 5	2.18E − 5	1.54E − 5	0.00E + 0	−1.54E − 5	−2.18E − 5	−1.54E − 5
0.54	0.00E + 0	2.34E − 5	3.31E − 5	2.34E − 5	0.00E + 0	−2.34E − 5	−3.31E − 5	−2.34E − 5
0.61	0.00E + 0	3.18E − 5	4.49E − 5	3.18E − 5	0.00E + 0	−3.18E − 5	−4.49E − 5	−3.18E − 5
0.69	0.00E + 0	4.05E − 5	5.72E − 5	4.05E − 5	0.00E + 0	−4.05E − 5	−5.72E − 5	−4.05E − 5
0.78	0.00E + 0	4.93E − 5	6.98E − 5	4.93E − 5	0.00E + 0	−4.93E − 5	−6.98E − 5	−4.93E − 5
0.88	0.00E + 0	5.59E − 5	7.90E − 5	5.59E − 5	0.00E + 0	−5.59E − 5	−7.90E − 5	−5.59E − 5
1.00	0.00E + 0	0.00E + 0	0.00E + 0	0.00E + 0	0.00E + 0	0.00E + 0	0.00E + 0	0.00E + 0

Note. The results are shown for (a) an 8×8 and (b) a 16×16 grid.

REFERENCES

1. P. Henrici, *Applied and Computational Complex Analysis* (Wiley, New York, 1974–1986), Vol. I, Chap. 5; Vol. III, Chaps. 16, 17.
2. J. P. Goedbloed, Conformal mapping methods in two-dimensional magneto-hydrodynamics, *Comput. Phys. Commun.* **24,** 311 (1981).
3. J. P. Goedbloed, Free-boundary high-beta tokamaks. II. Mathematical intermezzo: Hilbert transforms and conformal mapping, *Phys. Fluids* **25,** 2062 (1982).